Giant Star-shaped Nitrogen-doped Nanographenes

Juan P. Mora-Fuentes,[a] Alberto Riaño-Carnerero,[a] Diego Cortizo-Lacalle,[a] Akinori Saeki,[b] Manuel Melle-Franco,*[c] Aurelio Mateo-Alonso*[a,d]

[a] POLYMAT, University of the Basque Country UPV/EHU, Avenida de Tolosa 72, E-20018 Donostia-San Sebastian, Spain Fax: (+)34 943 50 6062 E-mail: amateo@polymat.eu

[b] Department of Applied Chemistry, Graduate School of Engineering, Osaka University Suita, Osaka 565-0871, Japan.

[c] CICECO - Aveiro Institute of Materials, Department of Chemistry, University of Aveiro 3810-193 Aveiro, Portugal

[d] Ikerbasque, Basque Foundation for Science E-48011 Bilbao, Spain

Abstract

Star-shaped nanographenes are large monodisperse polycyclic aromatic hydrocarbons that extend in size beyond the nanometer and have shown a lot of promise in a wide range of applications including electronics, energy conversion and sensing. Herein we report a new family of giant star-shaped N-doped nanographenes with diameters up to 6.5 nm. Furthermore, the high solubility of this SNG family in neutral organic solvents at room temperature allowed a complete structural, optoelectronic and electrochemical characterisation, which together with charge transport studies illustrate their n-type semiconducting character.

Nanographenes (NGs) are large monodisperse polycyclic aromatic hydrocarbons that extend in size beyond the nanometer and have shown a lot of promise in a wide range of applications including electronics, photonics, and energy.[1] Atomically-precise control over the NG structure is crucial to fully exploit their potential. For instance, by controlling the number of rings, their arrangement, heteroatom-doping and substitution, it is possible to fine-tune their energy levels and therefore, modulate electron affinities, ionization potentials, energy gaps, absorption and emission properties, among others.

Among these, planar threefold symmetric star-shaped nanographenes (SNGs), such as starphenes, cloverphenes and their extended derivatives (Figure 1),[2] have shown a prominent position as materials for charge transport, energy conversion and storage, light-emitting and sensing applications.[3] However, even if, there have been very impressive advances in recent years and large SNGs diameters reaching 3.0 nm (55 condensed rings) have been reported by solution synthesis,[2c-e, 2i-k] the largest soluble SNG that has been fully characterised presents a diameter of 2.8 nm (16 condensed rings).[2l] This is because of the lack of solubility of planar π systems that extend in two dimensions, which tend to aggregate strongly by π-stacking in solution (Figure 1). In fact, the synthesis of extended SNGs is still a challenging task that requires dealing with insoluble intermediates and products, which overall makes synthesis, purification, characterisation and processing difficult, slowing down the exploration of their fundamental properties and the development of potential applications.

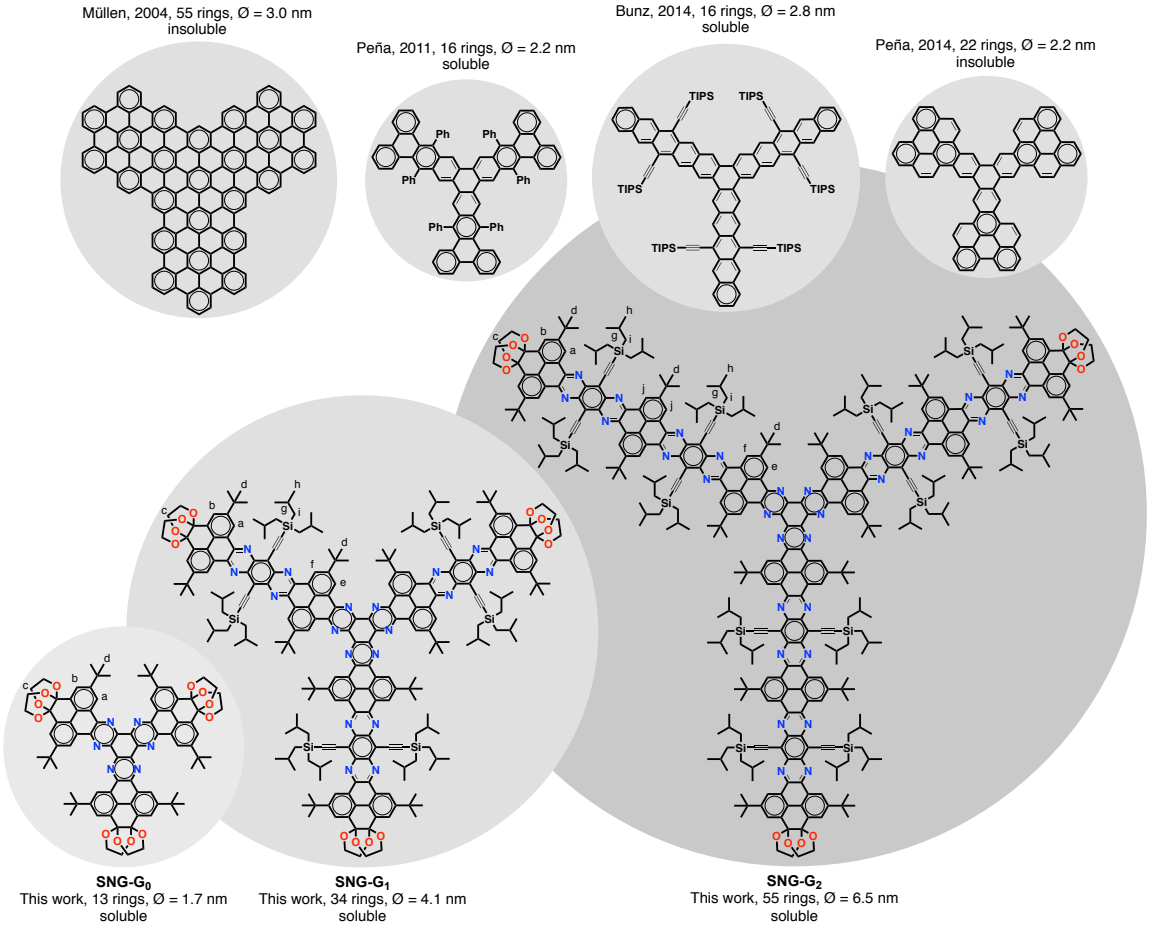

Figure 1. The SNG family (**SNG-G$_0$**, **SNG-G$_1$** and **SNG-G$_2$**) described in this work, in comparison to representative SNGs synthesised by solution methods.

Herein we report a new family of giant SNGs that show diameters exceeding those of the largest SNGs (3 nm) and that have been fully characterised thanks to their high solubility (Figure 1). For instance, the first generation of this family (**SNG-G$_1$**) shows a diameter of 4.1 nm (34 condensed rings), and remarkably, the second generation (**SNG-G$_2$**) shows a diameter of 6.5 nm (55 condensed rings). As we show below, the synthesis of this SNG family is not trivial and requires the careful design of a key C_3-symmetrical precursor (**SNG-G$_0$**), from which the aromatic core can be then extended radially. Furthermore, the high solubility of this SNG family in neutral organic solvents at room temperature allowed a complete structural, optoelectronic and electrochemical characterisation that together with charge transport studies illustrate their *n*-type semiconducting character.

On a first approach, we aimed at synthesising SNGs by cyclocondensation of precursor **A**[4] to the commercially available cyclohexane-1,2,3,4,5,6-hexaone (**HKT**) (Scheme 1a), which has been broadly used for the synthesis of hexaazatriphenylenes and hexaazatrinaphthylenes.[3a, 5] We selected precursor **A**, which consists on a dibenzodiazatetracene core with terminal protected ketones in the pyrene end and diamino groups at the quinoxaline end that enables an iterative reaction scheme, as it can be assembled with itself by a set of cyclocondensation/deprotection reactions. In addition, **A** possesses a combination of *tert*-butyl and tri-*iso*-butylsilyl (TIBS) groups that have proven to render large NGs soluble. However, when we carried out the cyclocondensation between building block **A** and **HKT** in the solvent mixtures typically used for this type of cyclocondensations, the reaction did not provide the expected cycloadduct **B** and instead, yielded an inseparable mixture of compounds. We exposed this mixture of compounds to Bunz oxidation conditions (MnO_2), which have proven to be useful to aromatise mildly incomplete dihydro intermediates of azaacenes and their derivatives,[6] and the mixture evolved to a major compound. Structural

characterisation of such compound confirmed the formation of linear C_2 ribbon-like condensation adduct **C** with 13 fused aromatic rings (Scheme 1a). Therefore, we can safely attribute the formation of **C** to the early formation of a mixture of dihydro species of the dicondensation product that was fully aromatised afterwards by MnO_2, in line with several cases that have been noted in recent literature.[7] The formation of the C_2 instead of the C_3 condensation was surprising since some of us reported the synthesis of the structurally equivalent hexa(TIBS)acetylene-substituted hexaazatrinaphthylene[8] and the reaction proceeded without problems to the desired product. Nevertheless, the formation of the C_2 condensation product can be rationalised in terms of both nucleophilicity and steric hinderance because of the lower nucleophilicity of the diamines on the quinoxaline residue of **A** in comparison to phenylenediamine derivatives, which are unable to overcome the steric hinderance of the C_3 condensation product.

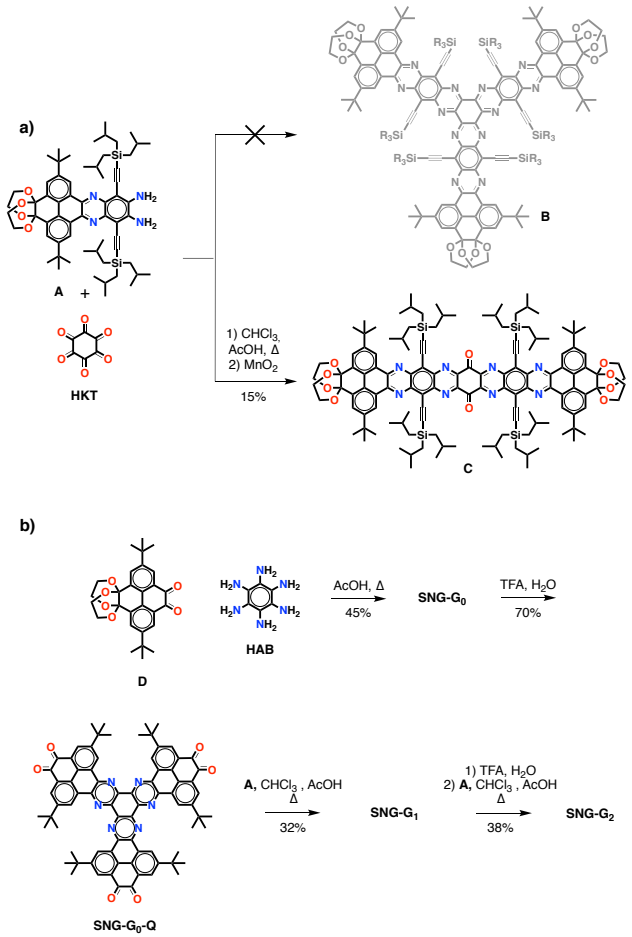

Scheme 1. a) Attempted synthesis of precursor **B**, leading to compound **C** instead. b) Synthesis of **SNG-G$_0$**, **SNG-G$_1$** and **SNG-G$_2$**.

At this stage, we changed strategy (Scheme 1b) and designed a new C_3 symmetrical precursor in which the three sets of diones are far apart from each other and at the same time are close to *tert*-butyl solubilizing groups that should not interfere sterically with the TIBS groups present at **A** during the triple cyclocondensation step. We therefore condensed pyrene diketone **D**[9] that can be obtained in 4 steps from pyrene and 1,2,3,4,5,6-hexaaminobenzene (**HAB**)[5] that can be obtained in 3 steps from 1,3,5-trichlorobenzene. The cyclocondensation proceeded without problems and yielded the hexaone-protected precursor **SNG-G$_0$** in a good yield (45%). The deprotection of the terminal *o*-diones in the presence of TFA and water yielded the hexaone-terminated precursor **SNG-G$_0$-Q** (70%). The cyclocondensation reaction between **A** and **SNG-G$_0$-Q** proceeded without any problems and yielded **SNG-G$_1$** after chromatographic purification (32%). The deprotection of the terminal diones in water/TFA, followed by cyclocondensation with **A** yielded the desired **SNG-G$_2$** (38%).

The whole SNG series were remarkably soluble in toluene, and chlorinated solvents at room temperature and we were able to establish unambiguously their structure by ^{1}H-NMR and ^{13}C-NMR spectroscopy and matrix-assisted laser desorption/ionization time of flight high-resolution mass spectrometry (MALDI-TOF HRMS). The ^{1}H-NMR and ^{13}C-NMR spectra showed remarkably sharp signals that allowed confirming the structure in all the SNGs, illustrating the high solubility of the whole series. For instance, the integration of ^{1}H-NMR signals are in agreement with the structures of the SNGs (Figure 2a), integrating 6 protons for the aromatic signals *a* and *b* in **SNG-G$_0$**, **SNG-G$_1$** and **SNG-G$_2$**, 6 protons for the aromatic signals *e* and *f* in the case of **SNG-G$_1$** and **SNG-G$_2$**, 12 protons for the aromatic signal *j* in the case of **SNG-G$_2$** (the assignments correspond to the lettering in Figure 1). While in **SNG-G$_0$**, **SNG-G$_1$** and **SNG-G$_2$**, 12 protons for the terminal diketal signals *c* were observed in all cases, which is also consistent with the structure.[10] Further evidence of the successful preparation of the SNGs came from MALDI-TOF HRMS that show ion peak masses

$(M+Ag)^+$ of 1553.5692, 4211.1790, and 6868.7884 Da, respectively for **SNG-G_0**, **SNG-G_1** and **SNG-G_2**, that matched with the expected mass. The isotopic distributions could be only recorded for **SNG-G_0** and **SNG-G_1** due to the high molecular weight of **SNG-G_2**, which is at the detection limit of the technique that illustrates the extremely high molecular weight of these monodisperse systems. Since we were not able to obtain single crystals suitable for X-ray diffraction, semiempirical quantum mechanics were used to investigate the structure of SNGs with the GFN-xTB method (Geometry, Frequency, Non-covalent, eXtended Tight-Binding) that allows computing efficiently high molecular weight systems with thousands of atoms.[4, 11] The simulations show that the SNG series can adopt a plethora of slightly twisted conformations as the result of the bulkiness and the TIBS groups (Figure S1), but that given the inherent flexibility of the *iso*-propyl substitutents the energies for interconversion between conformations is very small, which gives rise to nearly planar structures on average. The simulations show that the SNGs possess stable disk structures with diameters of 1.7, 4.1 and 6.5 nm respectively for **SNG-G_0**, **SNG-G_1** and **SNG-G_2**.

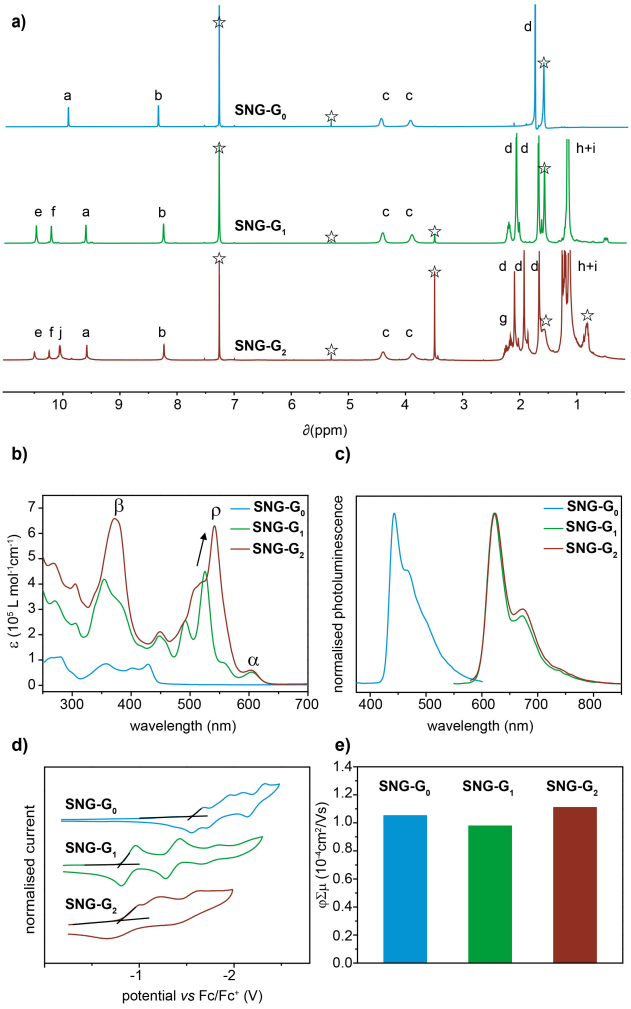

Figure 2. a) ^{1}H-NMR spectra in $CDCl_3$. The assignments correspond to the lettering in Figure 1. The stars indicate residual solvent peaks. b) UV-vis electronic absorption and c) photoluminescence spectra in $CHCl_3$. d) Cyclic voltammograms in an Ar-saturated 0.1 M solution of nBu$_4$NPF$_6$ in CH_2Cl_2. Potentials *versus* Fc/Fc$^+$. d) TRMC (λ = 355 nm, I_0 = 9.1 x 10^{15} photons/cm^2).

Thanks to the enhanced solubility, we could easily investigate the optoelectronic properties in solution. The absorption spectra of the SNGs were recorded in $CHCl_3$ and showed sets of absorption bands also consistent with their structure (Figure 2b). The electronic absorption spectrum of **SNG-G$_0$** is dominated by 3 bands at 357, 402 and 428 nm, with a molar attenuation coefficient of (68,429 $Lmol^{-1}cm^{-1}$) for the longest wavelength transition (Figure 2b). The absorption bands of **SNG-G$_1$** (354, 525 and 604 nm) and **SNG-G$_2$** (373, 541 and 605 nm) appear bathochromically shifted in comparison with those of **SNG-G$_0$** as consequence of the extension in the effective conjugation, which allows identifying three main absorption bands with their corresponding vibronic features. These were assigned as the α, ρ and β bands from longer to shorter wavelengths (Figure 2b), in agreement with previous assignments on pyrene-fused systems.[4, 11b, 12] The spectra showed that while the α band remains at almost invariable energies, the β and the ρ bands are increasingly shifted towards lower energies as a result of the radial extension of the π-system. Remarkably, also the molar absorptivity (ε) increases together with the diameter of the SNG, as exemplified by comparing the ρ bands of **SNG-G$_1$** (448,985 $Lmol^{-1}cm^{-1}$) and **SNG-G$_2$** (629,021 $Lmol^{-1}cm^{-1}$). The experimental electronic absorption spectra are in agreement with the calculated ones, which do not only corroborate the electronic structure but also shine light on the nature of the electronic transitions (Figure S2 and Table S1). In fact, time-dependent density functional theory (TD-DFT) and frontier orbital energies were computed with the 6-31g(d) basis set with the B3LYP Hamiltonian for **SNG-G$_0$-H**, **SNG-G$_1$-H**, and **SNG-G$_2$-H**, in which the TIBS groups on the on the acetylenes have been replaced by H atoms in order to reduce the calculation time due to the large size of the SNGs. A comparison of key electronic properties for both, GFN-xTB and B3LYP, Hamiltonians show that the differences due to this approximation are small and mostly negligible (Tables S2 and S3). The calculations show absorption spectra with the same trends as the experimental ones

in terms of energies and intensities, in which the spectrum of **SNG-G_0-H** also differs from the spectra of **SNG-G_1-H** and **SNG-G_2-H** (Figure S2). The first lower energy band in **SNG-G_1-H** and **SNG-G_2-H** – consistent with the experimental α band – originates from transitions between the degenerate HOMOs and LUMOs (Figure S4). The second band – consistent with the experimental ρ band – originates from the transitions between a set of lower energy non-frontier degenerate HOMO orbitals (HOMO–3 and HOMO–4 for **SNG-G_1-H**, and HOMO–6 and HOMO–7 for **SNG-G_2-H**) to the degenerate LUMOs (Figure S5).

Remarkably, all three SNGs are emissive regardless of their size and their photoluminescence spectra are also consistent with their electronic structure. The emission spectrum of **SNG-G_0** in $CHCl_3$ (λ_{ex} = 340 nm) exhibited a band at 443 nm (quantum yield (Φ) = 0.26[13]). Meanwhile, the photoluminescence spectra of **SNG-G_1** and **SNG-G_2** (λ_{ex} = 524 and 540 nm, respectively) in $CHCl_3$ show an isoenergetic emission band at 623 nm (Φ = 0.27 and 0.15,[14] respectively), since the emission originates in both cases from the α absorption band that is diameter independent. However, the emission of **SNG-G_1** and **SNG-G_2** is bathochromically shifted in comparison to **SNG-G_0**, as the result of the extended conjugation of the π-system.

The electrochemical properties of the SNGs were investigated by cyclic voltammetry in CH_2Cl_2 using $n$$Bu_4NPF_6$ (0.1 M) as electrolyte and ferrocene/ferrocenium (Fc/Fc^+) as internal standard (Figure 2d). The cyclic voltammograms show several reduction processes, while no oxidation processes were observed within the solvent-electrolyte window. From the cyclic voltammograms of **SNG-G_0** four reduction waves could be identified at potentials more negative than –1.5 V, while only three reduction waves at more positive potentials (between –0.5 and –2.0 V) were identified for **SNG-G_1** and **SNG-G_2**, in agreement with the extended conjugation. The three reduction waves are

broader and more anodically shifted in the case of **SNG-G$_2$**, which is consistent with both the extended conjugation and multiple degenerate LUMO orbitals (Figures S3-S5).

The energy levels were estimated from the electronic spectra and the cyclic voltammograms. We estimated the energy gaps (E_{gap}) from the absorption onset of the longest absorption wavelength with values of 2.78, 1.98 and 1.97 eV for **SNG-G$_0$**, **SNG-G$_1$** and **SNG-G$_2$**, respectively. These E_{gap} values follow the same trends as the theoretical values (B3LYP-6-311+g(2d,g)/B3LYP-6-31g(d)) of **SNG-G$_0$-H**, **SNG-G$_1$-H** and **SNG-G$_2$-H** (Tables S2 and S3). The LUMO levels (E_{LUMO}) were estimated from the onset of the first reduction potential (E_{LUMO} = –4.8–e(E_{ONSET}–$E_{1/2}^{Fc}$)). The E_{LUMO} of **SNG-G$_0$**, **SNG-G$_1$** and **SNG-G$_2$** were –3.24, –3.98 and –4.00 eV, respectively, which match reasonably well in absolute terms and very well in relative terms with the theoretical values (B3LYP-6-311+g(2d,g)/B3LYP-6-31g(d)) of **SNG-G$_0$-H**, **SNG-G$_1$-H** and **SNG-G$_2$-H** (Tables S2 and S3). The HOMO levels (E_{HOMO}) have been calculated from the difference between E_{LUMO} and E_g and were the following: –6.02, –5.96 and –5.97 eV for **SNG-G$_0$**, **SNG$_1$** and **SNG-G$_2$**, respectively.

To assess the charge transporting properties of SNGs, we performed time-resolved microwave conductivity measurements (TRMC)[15] directly on the solids powders (Figure 2e and Table S4). TRMC allows calculating the pseudo-photoconductivity values ($\varphi\Sigma\mu_{max}$), which can be considered the intrinsic or minimum charge carrier mobility of the material, without the need of contacts. For instance the $\varphi\Sigma\mu_{max}$ values correspond to the sum of the hole and electron mobilities ($\Sigma\mu$) times the quantum yield (φ). We obtained nearly invariable $\varphi\Sigma\mu_{max}$ values in the order of 10^{-4} cm^2 V^{-1} s^{-1} with average $\varphi\Sigma\mu_{max}$ values of 1.05 x 10^{-4}, 0.98 x 10^{-4} and 1.11 x 10^{-4} cm^2 V^{-1} s^{-1} for **SNG-G$_0$**, **SNG-G$_1$** and **SNG-G$_2$**, respectively, which are similar to those obtained for ribbon-like NGs,[4] π-gels[16] and conjugated polymers.[17] Similarly, nearly invariable half lifetimes ($\tau_{1/2}$) of 0.45, 0.65 and 0.50 μs for **SNG-G$_0$**, **SNG-G$_1$** and **SNG-G$_2$**,

respectively, were measured. The nearly invariable $\varphi\Sigma\mu$ and $\tau_{1/2}$ values observed are consistent with observed localized states.

In this work, we have reported the synthesis of highly soluble SNGs with diameters up to 6.5 nm (55 condensed rings), which doubles those of the largest SNGs. Their synthesis has been achieved by a careful design and synthesis of a C_3-symmetrical precursor from which the SNG core is then extended radially. Most importantly, this approach provides highly soluble SNGs, which has allowed their synthesis and purification by solution methods and also a full characterisation (^{1}H and ^{13}C NMR, HRMS, UV-vis, photoluminescence, cyclic voltammetry and TRMC) that show how the radial extension of the π-system results in changes in their electronic absorption, molar absorptivity, photoluminescence and electrochemistry, while other properties remain almost invariable, such as the photoluminescence of the higher SNGs and the charge transport properties. The high molar absorptivity, low LUMO energies and $\varphi\Sigma\mu$ values illustrate the *n*-type semiconducting character and their potential in charge transport and energy conversion applications.

Acknowledgements

We are grateful to the Basque Science Foundation for Science (Ikerbasque), POLYMAT, the University of the Basque Country (SGIker), Gobierno de España (Ministerio de Economía y Competitividad CTQ2016-77970-R and CTQ2015-71936-REDT), Gobierno Vasco (BERC program), Diputación Foral de Guipúzcoa (OF215/2016(ES)), the Portuguese Foundation for Science and Technology (IF/00894/2015) and CICECO - Aveiro Institute of Materials, POCI-01-0145-FEDER-007679 (FCT Ref. UID /CTM /50011/2013). This project has received funding from the European Union's Horizon 2020 research and innovation programme under grant agreement No 664878. This project has received funding from the European Research Council (ERC) under the European Union's Horizon 2020 research and innovation programme (grant agreement n° 722951).

References

[1] a) A. Narita, in *Synthetic Methods for Conjugated Polymers and Carbon Materials* (Eds.: M. Leclerc, J. Morin), Wiley-VCH, **2017**; b) A. Mateo-Alonso, *Chem. Soc. Rev.* **2014**, *43*, 6311-6324; c) A. Narita, X.-Y. Wang, X. Feng, K. Müllen, *Chem. Soc. Rev.* **2015**, *44*, 6616-6643; d) B. A. G. Hammer, K. Müllen, *Chem. Rev.* **2016**, *116*, 2103-2140; e) M. Stępień, E. Gońka, M. Żyła, N. Sprutta, *Chem. Rev.* **2017**, *117*, 3479-3716; f) Z. Cai, M. A. Awais, N. Zhang, L. Yu, *Chem* **2018**, DOI: 10.1016/j.chempr.2018.1008.1017.

[2] a) Z. Hua, W. Di, H. L. Sheng, Y. Jun, *Curr. Org. Chem.* **2012**, *16*, 2124-2158; b) E. Clar, A. Mullen, *Tetrahedron* **1968**, *24*, 6719-6724; c) V. S. Iyer, M. Wehmeier, J. D. Brand, M. A. Keegstra, K. Müllen, *Angew. Chem. Int. Ed.* **1997**, *36*, 1604-1607; d) J. Wu, Ž. Tomović, V. Enkelmann, K. Müllen, *J. Org. Chem.* **2004**, *69*, 5179-5186; e) Ž. Tomović, M. D. Watson, K. Müllen, *Angew. Chem. Int. Ed.* **2004**, *43*, 755-758; f) X.-Y. Cao, H. Zi, W. Zhang, H. Lu, J. Pei, *J. Org. Chem.* **2005**, *70*, 3645-3653; g) R. Rieger, M. Kastler, V. Enkelmann, K. Müllen, *Chem. Eur. J.* **2008**, *14*, 6322-6325; h) H.-P. Jia, S.-X. Liu, L. Sanguinet, E. Levillain, S. Decurtins, *J. Org. Chem.* **2009**, *74*, 5727-5729; i) Y. Zhang, D. Hanifi, S. Alvarez, F. Antonio, A. Pun, L. M. Klivansky, A. Hexemer, B. Ma, Y. Liu, *Org. Lett.* **2011**, *13*, 6528-6531; j) J. M. Alonso, A. E. Díaz-Álvarez, A. Criado, D. Pérez, D. Peña, E. Guitián, *Angew. Chem. Int. Ed.* **2012**, *51*, 173-177; k) B. Schuler, S. Collazos, L. Gross, G. Meyer, D. Pérez, E. Guitián, D. Peña, *Angew. Chem. Int. Ed.* **2014**, *53*, 9004-9006; l) E. C. Rüdiger, M. Porz, M. Schaffroth, F. Rominger, U. H. F. Bunz, *Chem. Eur. J.* **2014**, *20*, 12725-12728; m) C. Cheng, Y. Jiang, C.-F. Liu, J.-D. Zhang, W.-Y. Lai, W. Huang, *Chem. Asian J.* **2016**, *11*, 3589-3597; n) C.-F. Liu, C. Cheng, Y. Jiang, W.-Y. Lai, W. Huang, *New J. Chem.* **2017**, *41*, 13619-13624; o) J. Hieulle, E. Carbonell-Sanromà, M. Vilas-Varela, A. Garcia-Lekue, E. Guitián, D. Peña, J. I. Pascual, *Nano Lett.* **2018**, *18*, 418-423.

[3] a) J. L. Segura, R. Juárez, M. Ramos, C. Seoane, *Chem. Soc. Rev.* **2015**, *44*, 6850-6885; b) T. Wöhrle, I. Wurzbach, J. Kirres, A. Kostidou, N. Kapernaum, J.

Litterscheidt, J. C. Haenle, P. Staffeld, A. Baro, F. Giesselmann, S. Laschat, *Chem. Rev.* **2016**, *116*, 1139-1241; c) X.-Y. Yan, M.-D. Lin, S.-T. Zheng, T.-G. Zhan, X. Zhang, K.-D. Zhang, X. Zhao, *Tetrahedron Lett.* **2018**, *59*, 592-604; d) C. Peng, G.-H. Ning, J. Su, G. Zhong, W. Tang, B. Tian, C. Su, D. Yu, L. Zu, J. Yang, M.-F. Ng, Y.-S. Hu, Y. Yang, M. Armand, K. P. Loh, *Nat. Energy* **2017**, *2*, 17074; e) N. Wang, K. Zhao, T. Ding, W. Liu, A. S. Ahmed, Z. Wang, M. Tian, X. W. Sun, Q. Zhang, *Adv. Energy Mater.* **2017**, *7*, 1700522.

[4] D. Cortizo-Lacalle, J. P. Mora-Fuentes, K. Strutyński, A. Saeki, M. Melle-Franco, A. Mateo-Alonso, *Angew. Chem. Int. Ed.* **2018**, *57*, 703-708.

[5] D. Z. Rogers, *J. Org. Chem.* **1986**, *51*, 3904-3905.

[6] S. Miao, A. L. Appleton, N. Berger, S. Barlow, S. R. Marder, K. I. Hardcastle, U. H. F. Bunz, *Chem. Eur. J.* **2009**, *15*, 4990-4993.

[7] a) C. Wang, J. Zhang, G. Long, N. Aratani, H. Yamada, Y. Zhao, Q. Zhang, *Angew. Chem. Int. Ed.* **2015**, *54*, 6292-6296; b) D. Cortizo-Lacalle, C. Gozalvez, M. Olano, X. Sun, M. Melle-Franco, L. E. Hueso, A. Mateo-Alonso, *Org. Lett.* **2015**, *17*, 5902-5905.

[8] S. Choudhary, C. Gozalvez, A. Higelin, I. Krossing, M. Melle-Franco, A. Mateo-Alonso, *Chem. Eur. J.* **2014**, *20*, 1525-1528.

[9] R. García, M. Melle-Franco, A. Mateo-Alonso, *Chem. Commun.* **2015**, *51*, 8037-8040.

[10] ^{1}H-NMR does not show any evidence of the presence dihydro species during the cyclocondensation. For instance when **SNG-G$_2$** was exposed to Bunz oxidation conditions no change of colour was observed, which confirms that the aromatic core is fully aromatised.

[11] a) S. Grimme, C. Bannwarth, P. Shushkov, *J. Chem. Theory. Comput.* **2017**, *13*, 1989-2009; b) D. Cortizo-Lacalle, C. Gozalvez, M. Melle-Franco, A. Mateo-Alonso, *Nanoscale* **2018**, *10*, 11297-11301.

[12] E. Clar, *The Aromatic Sextet*, Wiley, London, **1972**.

[13] Estimated using 9,10-diphenylanthracene in hexane as a reference.

[14] Estimated using oxazine in MeOH as a reference.

[15] A. Saeki, Y. Koizumi, T. Aida, S. Seki, *Acc. Chem. Res.* **2012**, *45*, 1193-1202.

[16] M. Martínez-Abadía, G. Antonicelli, A. Saeki, A. Mateo-Alonso, *Angew. Chem. Int. Ed.* **2018**, *57*, 8209-8213.

[17] A. Saeki, S.-i. Ohsaki, S. Seki, S. Tagawa, *J. Phys. Chem. C* **2008**, *112*, 16643-16650.